View metadata, citation and similar papers at core.ac.uk

brought to you by CORE

provided by Digital.CSIC

This is the last draft sent to the Editorial by the authors of the article:

M. GÓMEZ, S. F. MEDINA and G. CARUANA
"Modelling of Phase Transformation Kinetics by Correction of Dilatometry Results for a Ferritic Nb-microalloyed Steel"

ISIJ International
Vol. 43 (2003), No. 8, pp. 1228–1237
ISSN: 0915-1559
DOI: 10.2355/isijinternational.43.1228

To be published in Digital.CSIC, the Institutional Repository of the Spanish National Research Council (CSIC)

See more papers from the authors on:

http://digital.csic.es

http://www.researcherid.com/rid/B-7922-2008

Modelling of phase transformation kinetics by correction of dilatometry results for a ferritic Nb-microalloyed steel

M. GÓMEZ, S. F. MEDINA, G. CARUANA

National Centre for Metallurgical Research (CENIM-CSIC), Av. Gregorio del Amo 8, 28040-Madrid, Spain

E-mail: smedina@cenim.csic.es

Using the dilatometry technique, $\gamma \rightarrow \alpha$ transformation kinetics has been determined at different cooling rates in a steel with low carbon and low niobium contents (0.09 and 0.017 mass% respectively). First of all the real and the conventional transformation temperatures of the steel were determined. The real start temperature for proeutectoid ferrite formation (A'_{r3}) corresponds to the point where the dilatometric curve starts to diverge from the straight during cooling. The conventional start and finish temperatures for proeutectoid ferrite formation (A_{r3} and A_{r1}) are given by two points close to the minimum and the first maximum of the curve, respectively. The real start and finish eutectoid transformation temperatures –$(A'_{r1})_s$ and $(A'_{r1})_f$– correspond to the second point of inflection and a point close to the second relative maximum of the curve, respectively. Carbon enrichment of the remaining austenite, as the transformation to ferrite advances, is corrected taking into account the dependence on the carbon content of the atomic volume of austenite. On the other hand, the dilatometric data have also been corrected with regard to the different expansion coefficients of austenite and ferrite. In this way it has been seen that the lever-rule method applied to the dilatometric curve is useful for determining transformation temperatures, but not for determining transformation kinetics, since the amount of proeutectoid ferrite calculated with this method was up to 10% greater than the real amount measured with an image analyser. Finally a model based on Avrami's law has been developed for the real $\gamma \rightarrow \alpha$ transformation kinetics.

KEY WORDS: microalloyed steel, dilatometric analysis, phase transformations, kinetics, microstructure, modelling.

1. Introduction

Phase transformations are one of the factors that most influence steel properties, especially the $\gamma \rightarrow \alpha$ transformation. The transformation kinetics of proeutectoid ferrite in continuous cooling has been studied by several authors. The percentages of austenite transformed to different phases (ferrite, pearlite, bainite) have been charted in continuous cooling transformation (CCT) diagrams, where the evolution of the fraction transformed to ferrite suggests that this can be predicted by an Avrami type law. [1-4)]

Dilatometry is one of the classic techniques, along with differential thermal analysis and quantitative analysis of microstructures, most commonly used to determine the start and end of phase transformations in steels.

The dilatometric technique may be applicable in the study of phase transformation kinetics in steels if a relationship can be established between the transformed phase fractions, the temperature, the phase compositions and dilatation, [5)] i.e. taking into account the redistribution of carbon between the transformed ferrite and the remaining austenite and their different expansion coefficients. So, standard data analysis based on the lever-rule method is not usually appropriate to accurately determine the different phase volume fractions when several phases are formed. In this case only the start temperature of the first transformation and the end temperature of the final transformation are relevant. [6)] This is the case with carbon steels, where this method is not applicable for two reasons: [7-9)] (a) carbon is redistributed between the forming ferrite and the remaining austenite, increasing the specific volume of austenite;

and (b) the formation of pearlite has a distinctly different volume effect to the formation of ferrite.

Though many studies involving dilatometric tests continue to apply the lever rule as a quick method for knowing the transformation kinetics of proeutectoid ferrite in cooling, [10] many other authors correct the dilatometric curve in order to avoid the errors that arise if the aforementioned aspects are not taken into account. [11-13] These authors apply several calculation methods, and it is here where differences between the results are found.

On the other hand, when the transformation takes place in isothermal conditions the transformed ferrite fraction as a function of time obeys Avrami's law. [14,15] When the transformation takes place in continuous cooling conditions the transformation kinetics also seem to obey Avrami's law, provided that the cooling rate is constant, since in this case there would be a linear equivalence between temperature and time, and zero time would correspond to the A_{r3} transformation temperature. [16,17]

This paper studies the kinetics of the austenite to proeutectoid ferrite transformation as determined by dilatometric analysis. The effects of carbon enrichment of the austenite and overlapping of the different thermal contractions of the two phases are corrected applying the method reported by Kop et al. [13]

2. Experimental procedure

The steel used was manufactured by electroslag remelting (ESR) in a laboratory unit capable of producing 30 kg ingots. Its cast chemical composition is shown in **Table**

1. This technique avoids macrosegregation, both in alloying elements and impurities, and there is considerably less microsegregation; these defects being present in conventional ingots and continuous casting billets. [18)]

The decomposition of austenite in continuous cooling has been analysed using an Adamel DT 1000 high resolution dilatometer. The specimens for dilatometry had a radius of 1 mm and a length of 12 mm. The material used in the tests was as-cast in order to ensure that the specimen composition was exactly as shown in Table 1.

During testing the specimens were protected from oxidation by a vacuum of the order of 10^{-5} MPa. The heating rate was 1 ºC/s, the austenitisation temperature 1000ºC (1273 K), the holding time 2 min and the cooling rates 0.25, 0.42, 0.84 and 1.25 ºC/s, respectively.

Finally, with the aim of verifying the transformation kinetics model and the errors committed by applying the lever rule, the phases present (ferrite and pearlite) were counted by image analysis using version 6.1 Optimas software.

3. Theory on correction of the dilatometric curve

The theory used in this work to correct the dilatometric curve in order to calculate the transformed fraction in ferritic-pearlitic steels has been reported by Kop et al. [13)] and is summarised as follows.

When a material undergoes a phase transformation its lattice structure changes and this is accompanied by a change in the specific volume. In the case of a pure iron

specimen, cooling from temperatures above A_{r3} causes the austenite, which has a f.c.c structure, to transform into ferrite, which has a less closely packed b.c.c structure. This phase transformation will cause a volume expansion of about 1.6%.

In the case of steel the lattice transformation also takes place, but in addition there is a redistribution of the alloying elements. The consideration of *paraequilibrium* [19] can be taken as a good approach for the kinetics of this transformation. In this case there is insufficient time for the partitioning of substitutional solute atoms to occur and the adjoining phases have identical X/Fe atom ratios, where X represents the substitutional solute elements. However, interstitial solutes such as carbon are able to partition and attain equilibration of the chemical potential in both phases. [14]

During the transformation the austenite will gradually transform into ferrite, in which the maximum solubility of carbon is limited, and the remaining austenite will become carbon-enriched. Both the formation of ferrite and the carbon-enrichment of austenite cause the specimen to expand. In order to delimit the total amount of ferrite transformed in cooling, the formation of ferrite and pearlite is assumed to take place in separate temperature regions, as can be expected from the equilibrium phase diagram. The second point of inflection on the cooling dilatometric curve indicates an increased transformation rate, as is expected at the start of the pearlite formation.

The atomic volume of a specimen is determined by the fractions of the phases present multiplied by their atomic volume, from the equation:

$$V(T) = \sum_i f_i V_i(T) \text{ .....} \textbf{(1)}$$

where V is the average atomic volume of the specimen, V_i is the atomic volume of phase *i*, f_i is the volume fraction of phase *i*, and *T* is the temperature. In low alloy steels, especially low carbon steels, and when cooling rates are less than approximately 5 ºC/s, the transformed phases are ferrite and pearlite. The atomic volumes (V_i) are related to the lattice parameters by the following expressions:

$$V_\alpha = \frac{1}{2}a_\alpha^3;\ V_\gamma = \frac{1}{4}a_\gamma^3;\ V_p = (1-\rho)V_\alpha + \rho V_\theta$$

with $V_\vartheta = \frac{1}{12}a_\theta b_\theta c_\theta$ and ρ the cementite fraction in the pearlite. The structure of cementite (Fe_3C) is orthorhombic and contains 12 iron and 4 carbon atoms.

Table 2 shows the lattice parameters of ferrite (α), austenite (γ) and cementite (θ) as a function of the temperature T and the atomic fraction of carbon (ξ), according to the literature. [7,20-23)]

Equation (1) would be difficult to apply if the different phases –in this case ferrite and pearlite– were to form simultaneously, and though in practice this could occur in a certain temperature interval, where the cooling rate would be decisive, we assume that at the cooling rates applied in this work, pearlite will start to be transformed once all the proeutectoid ferrite has been formed, as has been mentioned above.

Therefore at high temperatures, at the start of the austenite to ferrite transformation, the ferrite fraction is given by:

$$f_\alpha = \frac{V - V_\gamma}{V_\alpha - V_\gamma} \text{ ……}\textbf{(2)}$$

and until the start of the eutectoid transformation, $f_\alpha + f_\gamma = 1$.

Equation (2) will be resolved by calculating the specific atomic volumes of austenite (V_γ) and ferrite (V_α), according to the expressions given in Table 2.

In steels whose microstructure is formed by ferrite and pearlite, once the ferrite has been quantified by applying the above equations the resulting phase will obviously be pearlite. The pearlite fraction as a function of the temperature is calculated in the following way: [13)]

$$f_p = \frac{V - V_\gamma + f_\alpha (V_\gamma - V_\alpha)}{V_p - V_\gamma} \text{ ……}\textbf{(3)}$$

On the other hand, during the pearlite transformation only pearlite can be assumed to form, and this means that the ferrite fraction f_α is constant and that no further austenite enrichment occurs, with the volume of austenite being only temperature-dependent.

The total atomic volume (V) is calculated from the dilatometric curve in the following way, where it is supposed that the expansion/contraction is isotropic:

$$\frac{\Delta L}{L_0} = \frac{\Delta V_s}{3V_{0,s}} = \frac{\Delta V}{3V_0} \text{ ……..}\textbf{(4)}$$

where:

ΔL = measured length change of specimen

L_0 = initial length of specimen

ΔV_s = volume change of specimen

$V_{o,s}$ = initial volume of specimen

ΔV = atomic volume change (V-V_0)

V_0 = initial average atomic volume

In order to introduce the expansion measured by dilatometry ΔL in equation (2), the average atomic volume V can be written as:

$$V = kV_0\left(\frac{3\Delta L}{L_0}+1\right) \text{……..} \textbf{(5)}$$

where k is a scaling factor whereby once the austenite/ferrite transformation starts, the volume V coincides with the volume V_γ. This factor is ideally equal to 1. However, due to non-isotropic effects in the contraction of the specimen during cooling or errors in the signal from the dilatometer, the factor k may differ slightly from 1. To compensate for such effects, the factor k is introduced in equation (5). The scaling factor can be determined by considering the dilatation signal just before (equations 1 and 5 with f_γ =1) and after (equations 3 and 5 with $f_\alpha = (f_\alpha)_{eq}$ and $f_p = (f_p)_{eq}$ the transformation. Due to the lack of detailed information on transformation–plasticity effects, the scaling factor is varied linearly between the values found directly before and after the transformation.

4. Results and discussion

4.1. Dilatometric curves, microstructures and application of the lever rule

The dilatometry specimens were subjected to the tests indicated above. It is important to note that all the specimens were austenitised at the same temperature (1000ºC), that the heating rate was always the same (1 ºC/s), that the holding time at this temperature was also the same, and finally that each specimen was cooled at a different rate.

Figures 1(a,b)-4(a,b) show the dilatometric curves obtained from the tests, along with the corresponding ferrite and pearlite microstructures. On each dilatometric cooling curve an indication is made of the different critical transformation temperatures which may be deduced from the curves and whose meaning is as follows: [16-24)]

A'_{r3} = Real transformation start temperature for proeutectoid ferrite formation

A_{r3} = Conventional or apparent transformation start temperature for proeutectoid ferrite formation

A_{r1} = Conventional or apparent transformation final temperature for proeutectoid ferrite formation

$(A'_{r1})_s$ = Real transformation start temperature for pearlite formation

$(A'_{r1})_f$ = Real transformation final temperature for pearlite formation

All the critical transformation temperatures have been determined with the assistance of the first derived function and the second derived function, since they are more sensitive to changes in the slope than the dilatometric curve itself. The A'_{r3}

temperature is given by the point on the dilatometric curve where the straight line starts to gradually diverge from the straight during cooling. The A_{r3} temperature is given by the point close to the minimum of the dilatometric curve, i.e. a point where the change in the slope starts to be more important. The A_{r1} temperature is also given by a point close to the first maximum of the dilatometric curve. Finally, the critical temperatures $(A'_{r1})_s$ and $(A'_{r1})_f$ are given by the second point of inflection and by a point close to the second relative maximum of the dilatometric curve, respectively.

It is well known that the pearlitic transformation occurs instantaneously under equilibrium conditions and for a Fe-C steel without other alloying elements this temperature would be close to 723ºC. Therefore, what should occur in practice is that the length of the temperature interval $(A'_{r1})_s$ - $(A'_{r1})_f$ where the pearlitic transformation takes place during cooling should tend to drop towards zero as the cooling rate decreases. In order to confirm this, the values of $(A'_{r1})_f$ and $(A'_{r1})_s$ have been shown against the cooling rate **(Figure 5)** and it can be seen that the regression lines of both critical temperatures meet at a point that corresponds to a temperature of approximately 707ºC and a cooling rate of approximately 0.005 ºC/s. It is therefore deduced that equilibrium conditions are achieved at this cooling rate. On the other hand, the temperature of 707ºC represents the eutectoid transformation temperature that would correspond to the studied steel if it were cooled very slowly, in conditions close to equilibrium conditions. Its value which is lower than the theoretical value of 723ºC from the Fe-C diagram is obviously due to the Mn content, since this element is known to lower the A'_{r3} temperature of the start of the $\gamma \rightarrow \alpha$ transformation and also the $(A'_{r1})_s$ temperature of the start of the eutectoid transformation.

The critical transformation temperature values thus determined are shown in **Table 3**. The cooling rate affects all the critical temperatures, and a notable drop in the latter is observed as the cooling rate increases. Similarly, the pearlitic transformation interval given by $\{(A'_{r1})_s - (A'_{r1})_f\}$ is reduced as the cooling rate decreases, since at its limit, close to equilibrium conditions, this interval should be zero.

Applying the lever rule it is possible to know the transformation kinetics, though this method involves a certain error, as has already been noted. **Figure 6** presents a scheme of the application of the lever rule for a dilatation curve during cooling (solid line). In this figure, the dash straight lines represent the extrapolated dilatations of austenite phase (lower line) and the mixed ferrite/pearlite phase (upper line). Segment *x* results from the subtraction of the lower straight line from the dilatation curve, and *y* is the subtraction of the dilatation curve from the upper straight line. In this way, the transformed fraction will be given by the expression:

$$f = \frac{x}{x + y} \quad \textbf{.....(6)}$$

which is equal to the ratio of the apparent dilatation change to the maximum possible dilatation change. The extrapolated dilatation lines are calculated by regression of the dilatometric data, which facilitates the calculation of equation (6) and allows good precision to be obtained in the measurements of the *x* and *y* segments.

The application of equation (6) to the above dilatometric curves gave the results shown in **Figures 7-10**, respectively, in which the transformed fraction curve has been plotted as a function of the temperature corresponding to each cooling rate. It has been

attempted to make the graphs sufficiently descriptive, and in this sense the transformed fraction percentages corresponding to each critical transformation temperature have been indicated. According to the graphs, the pearlite percentage was 3% for the cooling rates of 1.25, 0.84, 0.42 ºC/s and 4% for the cooling rate of 0.25 ºC/s. These values are considerably lower than those observed at a glance in the microstructures of Figures 1(b)-4(b).

4.2. Ferrite and pearlite percentages measured by image analyser

The ferrite and pearlite percentages corresponding to the above microstructures were measured by an image analyser. Measurements were made using several micrographs prepared at x200 magnification and the values noted for each cooling rate represent the average for the different images analysed. The images may be considered to be two-phase, in which the “black phase” represents the pearlite plus the ferritic grain boundaries, and thus after grey-level discrimination it was necessary to filter the image to remove the grain boundaries.

The pearlite and ferrite percentages **(Table 4)** are each very similar for the three highest cooling rates, close to 11.5% for pearlite and 88.5% for ferrite. However, at the cooling rate of 0.25 ºC/s, the pearlite percentage was 18% and the ferrite percentage was 82%. This difference is believed to be due to the fact that the dilatometry specimens were machined directly from the ingot, i.e. as-cast, and the inherited dendritic microsegregation has favoured the formation of pearlite in the interdendritic sites, which are richer in solutes, especially when the cooling rate is lower. On the other hand, the small dimensions of the dilatometry specimens may have been influential in making the volumes or percentages of the interdendritic zone different, which would contribute to

the formation of a greater or smaller amount of pearlite. In any case, the directly measured percentages are much greater, approximately three times greater, than those calculated by applying the lever rule to the dilatometric curves. This means that the error which is committed in applying the lever rule to calculate the transformed fractions is too great and needs to be corrected.

It should be recalled that the error committed by applying the lever rule would have been even greater if the studied steel had had a higher carbon content, reaching a maximum for an atomic fraction carbon of approximately 2.5, and the ferrite percentage given by the lever rule would have been twice the real percentage. [13)]

4.3. Correction of dilatometric data

The use of **equation (5)** to calculate the real fraction of transformed proeutectoid ferrite as a function of the temperature requires a certain methodology which facilitates the calculation of V as a function of the temperature. First of all the volume V should coincide with V_γ when the austenite-ferrite transformation starts, i.e. when the A'_{r3} temperature is reached. In this way **equation (2)** will give a zero value for f_α when this temperature is reached.

With the aim of facilitating computer calculations, the initial average atomic volume (V_0) has been taken as the atomic volume of austenite (V_γ) for a standard temperature of 950ºC, irrespective of the cooling rate used and of the critical temperatures of the start and end of the transformation (A'_{r3} and $(A'_{r1})_f$) obtained. On the other hand, it has been established that for this temperature the value $\frac{\Delta L}{L_0}$ is zero.

With these two initial hypotheses the values of k in the austenitic region (k_γ) and in the pearlitic region (k_α) have been slightly lower than 1 in all cases.

If the temperature selected to calculate V_0 from V_γ were any other greater than or equal to A'_{r3}, the fractions calculated (f_α and f_p) would be the same, there only being a variation in an equal proportion of the values of k_γ and k_α. This would also be true if V_0 were defined as the atomic volume for $T = (A'_{r1})_f$ considering ($f_\alpha = f_\alpha^{eq}$ and $f_p = f_p^{eq}$).

Modification of the temperature for which $\frac{\Delta L}{L_0} = 0$ also has no significant influence on the final results of the calculations of the transformed fraction. It may be noted that if A'_{r3} is taken as the temperature for which $V = V_0$ and $\frac{\Delta L}{L_0} = 0$, this would give $k_\gamma = 1$. Similarly, if the selected temperature is $(A'_{r1})_f$, this would give $k_\alpha = 1$.

In any case, the atomic volume V calculated from **equation (5)** must coincide with V_γ when the austenite-ferrite transformation starts, i.e. when the A'_{r3} temperature is reached. In this way **equation (2)** will give a zero value for f_α when this temperature is attained. At that moment all the carbon contained in the steel (0.09 wt.% = 0.42 at.%) is in the austenite. As the temperature decreases, the austenite will be transformed into proeutectoid ferrite, which will reject part of the carbon away to the non-transformed austenite. This carbon enrichment of the austenite is a function of the ferrite fraction at each moment, for which **equation (2)** must be resolved by means of an iterative process based on Newton's method. This iterative calculation will be carried out for each of the points on the dilatometric curve up to the $(A'_{r1})_s$ temperature, after which it is assumed

that ferrite ceases to form and only pearlite is formed. At temperatures below $(A'_{r1})_s$ there is no carbon enrichment of the austenite, and therefore V_γ only depends on the temperature and it is no longer necessary to carry out the iterative process. The pearlite fraction will easily be obtained from **equation (3)**, bearing in mind that the values of f_α, of the carbon concentration in the austenite (ξ) and of the cementite ratio in the pearlite (ρ) remain constant.

In this way the transformed fractions of proeutectoid ferrite between A'_{r3} and $(A'_{r1})_s$ and of pearlite between $(A'_{r1})_s$ and $(A'_{r1})_f$ were determined. The results are shown in **Figures 11-14**, corresponding respectively to the different cooling rates, in which the transformation curves calculated by applying the lever rule have also been plotted. Comparison of the two curves shows that at the start of the transformation the error which is committed when applying the lever rule is practically negligible, and that the two curves start to diverge once the transformed fraction has reached 30%. The absolute error that is committed when applying the lever rule is maximum when the $(A'_{r1})_s$ temperature is reached, i.e. when the proeutectoid ferrite transformation has ended and the pearlitic transformation starts.

Table 4 sets out the total ferrite and pearlite fractions determined by the image analyser (IA), the fractions calculated by the lever rule (LR) and the fraction yielded by iterative calculation of the atomic volume of austenite (Kop's method). **Figure 15** illustrates these values as a function of the cooling rate. The values determined by the image analyser and by iterative calculation are seen to be very similar, and it should not be forgotten that the former represent an experimental measurement of good accuracy, with an estimated error of less than 1%.

The relative error in the lever rule results, to calculate the total proeutectoid ferrite fraction at $(A'_{r1})_s$, is defined by

$$\varepsilon=(X_{LR}-X_{Kop})/X_{Kop}$$

where, X_{LR} is the fraction obtained from the lever-rule approach and X_{Kop} the fraction determined by iterative calculation according to Kop's method..

The value of ε was approximately 10%, irrespective of the cooling rate. This coincides with the results reported by Kop et al. [13], whose error versus carbon percentage curve gives a similar result for a steel of the same carbon content as that used in this work (0.42 at.%).

In general, the lever rule always gives a higher ferrite percentage than that which is really obtained, irrespective of the steel's carbon content, since it cannot distinguish between the dilatation experienced by the specimen due to the formation of ferrite and the dilatation experienced by the austenite due to progressive carbon enrichment.

4.4. $\gamma \rightarrow \alpha$ transformation kinetics

When the dilatometric test is carried out at a constant cooling rate, as has been the case in the present work, the temperature variable is directly proportional to the time variable, giving $t=T/\theta$, where θ would be the cooling rate.

As has been seen above in **Figures 11-14**, the transformation curves, both that determined by the lever rule and that calculated, present two perfectly differentiated zones, namely that corresponding to the austenite to proeutectoid ferrite transformation, between the critical temperatures A'_{r3} and $(A'_{r1})_s$, and that corresponding to the transformation of the remaining austenite into pearlite, between $(A'_{r1})_s$ and $(A'_{r1})_f$. When the two transformations take place in isothermal conditions they occur by nucleation and growth, and therefore in principle they could be predicted by an Avrami type equation. [25)] A model of transformation kinetics in isothermal conditions may be converted to non-isothermal transformation kinetics, for instance in continuous cooling, if the expression for the nucleation rate and the growth rate is known, in both cases as a function of the temperature. [26)] Differentiation of the Avrami equation, introducing the cooling law, and its subsequent integration would give an Avrami equation as a function of time for non-isothermal conditions.

Bearing the above in mind, the following Avrami expression has been used to model the $\gamma \rightarrow \alpha$ transformation:

$$X_\alpha = 1\text{-}exp\ [-ln2\ (t/t_{0.5})^n] \quad \textbf{(7)}$$

where $t_{0.5}$ is the time necessary to reach 50% of the ferritic volume.

Equation (7) recalls the expression used for other physical phenomena that take place by nucleation and growth, as is the case of recrystallisation. [27)] The advantage of **equation (7)** over other Avrami expressions [28)] lies in the introduction of the parameter $t_{0.5}$ which replaces the nucleation and growth rates with a single parameter and

facilitates modelling, since it may be expressed as a function of other variables such as the cooling rate, austenite grain size, steel chemical composition and temperature. [27)]

In order to predict the kinetics of the $\gamma \rightarrow \alpha$ transformation it is therefore necessary to determine the values of $t_{0.5}$ and n in equation (7). To this end X_α has been represented versus time, taking as the origin ($t=0$) the moment at which the transformation starts, i.e. when the A'_{r3} temperature is reached. The $\gamma \rightarrow \alpha$ transformation ends at the $(A'_{r1})_s$ temperature, at which moment 100% of the proeutectoid ferrite is obtained. Thus in order to plot the proeutectoid ferrite fraction versus time it is sufficient to represent the fraction corrected by the iterative calculation as a function of time, rationalising the representation up to 100%. The result is shown in **Figure 16**, which represents the proeutectoid ferrite fraction as a function of time for each of the cooling rates. The parameter $t_{0.5}$ and the exponent n are calculated by means of regression of the points (t, X_α) according to equation (7). Both of these magnitudes may also be calculated by converting equation (7) into a linear equation applying logarithms and subsequently by linear regression of the points (t, X_α). The values obtained for the parameter $t_{0.5}$ and the exponent n corresponding to each cooling rate are shown in Table 5. The value of n may be considered to be constant, since the small variations that are found are not significant. The value of the parameter $t_{0.5}$ obviously varies with the cooling rate and its representation versus the inverse of the cooling rate is shown in **Figure 17**, obviously giving a straight line since the cooling rate in each test remained constant throughout the cooling.

Expression (7) has also been represented in **Figure 16**, where a good prediction of the proeutectoid ferrite transformation kinetics is observed, except at the start of the transformation.

Finally, the pearlitic transformation is of little interest in this steel, since the amount of pearlite is much smaller than the amount of ferrite and has hardly any influence on its mechanical properties. [29)]

5. Conclusions

1. The dilatometric curve is very useful for determining the critical transformation temperatures, but is not appropriate for directly determining, by means of the lever rule, the kinetics of the phase transformations.
2. The kinetics of both the austenite/proeutectoid ferrite transformation and of the retained austenite/pearlite transformation may be determined with good approximation from the dilatometric curve, making the appropriate corrections according to the method of Kop et al.
3. The error that would be committed by applying the lever rule to determine the total proeutectoid ferrite fraction would be 10% in this steel. The relative error in the determination of the amount of pearlite is much greater, approximately 75%.
4. The total fractions of proeutectoid ferrite and pearlite determined by the method of Kop et al. coincided almost exactly with the fractions determined experimentally by image analysis. This confirms that the method of Kop et al. is suitable for determining the real transformation kinetics.
5. The kinetics of the austenite/proeutectoid ferrite transformation in cooling may be predicted by an Avrami equation, whose exponent *n* has an approximate value of 2.

6. Cooling rates of less than 0.005 ºC/s approach equilibrium conditions in which the eutectoid transformation (retained austenite→pearlite) occurs at a temperature of 707ºC.

Acknowledgements

The authors would like to thank the I3P Program of CSIC, financed by the European Social Fund, for the funding of the grant of Eng. M. Gómez.

REFERENCES

1) R. Bengochea, B. López and I. Gutiérrez: *Metall. Mater. Trans. A*, **29** (1998), 417.

2) V.M. Khlestov, E.V. Konopleva and H.J. Mcqueen: *Mater. Sci. Technol.*, **14** (1998), 783.

3) G.P. Krielaart, J. Siestma and S. Van Der Zwaag: *Mater. Sci. Eng.*, **A237** (1997), 216.

4) R.A. Vandermeer: *Acta Metall. Mater.*, **38** (1990), 2461.

5) J.Z. Zhao, C. Mesplont and B.C. De Cooman: ISIJ Int., **41** (2001), 492.

6) C. Mesplont, J. Z. Zhao, S. Vandeputte and B.C. De Cooman: *Steel Res.*, **72** (2001), 263.

7) M. Onink, F.D. Tichelaar, C.M. Brakman, E.J. Mittemeijer and S. Van der Swaag: *Z. Metallkd.*, **87** (1996), 24.

8) M. Takahashi and H.K.D. Bhadeshia: *J. Mat. Sci. Lett.*, **8** (1989). 47.

9) T.A. Kop, J. Sietsma and S. Van Der Zwaag: Proc. Materials Solutions ’97 on Accelerated Cooling/Direct Quenching Steels, ASM International, Materials Park, Ohio, (1997), 159.

10) R. Pandi, M. Militzer, E.B. Hawbolt and T.R. Meadowcroft: Proc. Int. Symp. on Phase Transformations during the Thermal/Mechanical Processing of Steels, Vancouver, Ed. By E.B. Hawbolt and S. Yue, The Metallurgical Society of the Canadian Institute of Mining, Metallurgy and Petroleum (CIM), Montreal, Quebec, (1995), 459.

11) G. Pariser, P. Schaffnit, I. Steinbach and W. Bleck: *Steel Res.*, **72** (2001), 354.

12) J.Z. Zhao, C. Mesplont and B.C. De Cooman: *ISIJ Int.*, **41** (2001), 492.

13) T.A. Kop, J. Sietsma, S. Van Der Zwaag: *J. Mat. Sci.*, **36** (2001), 519.

14) C. Capdevilla, F.G. Caballero and C. García de Andrés: *Metall. Mater. Trans. A*, **32** (2001), 661.

15) R.C. Reed and H.K.D.H. Bhadeshia: *Mater. Sci. Technol.*, **8** (1992), 421.

16) S.F. Medina, M.I. Vega and M. Chapa: *Mater. Sci. Technol.*, **16** (2000),163.

17) R. Bengoechea, B. López and I. Gutierrez: *Metall. Mater. Trans. A*, **29** (1998), 417.

18) S.F. Medina and A. Cores: *ISIJ Int.*, **33** (1993), 1244.

19) H.K.D.H. Bhadeshia: *Progr. Mater. Sci.*, **29** (1985), 321.

20) H. Stuart and N. Ridley: *JISI*, **204** (1966), 711.

21) R. C. Reed and J. H. Root: *Scr. Mater.*, **38** (1998), 95.

22) M. Onink, C.M. Brakman, F.D. Tichelaar, E.J. Mittemeijer and S. Van der Swaag: *Scr. Metall. Mater.*, **29** (1993), 1011.

23) C. Qui and S. Van der Swaag: *Steel Res.*, **68** (1997), 32.

24) E.A. Wilson and S.F. Medina: *Mater. Sci. Technol.*, **16** (2000), 630.

25) 25) R. E. Reed-Hill: Physical Metallurgy Principles, Ed. by R.E. reed-Hill & R. Abbaschian, 3rd edition, PWS-Kent Publishing Company, Boston, (1992).

26) A. Roosz, Z. Gacsi and E.G. Fuchs: *Acta Metall.*, **31** (1983), 509.

27) C.M. Sellars: Hot Working and Forming Processes, ed. by C.M. Sellars and G.J. Davies, Metals Society, London (1980), 3.

28) M. Avrami: J. Chem. Phys., **8** (1940), 212.

29) F.B. Pickering: Physical Metallurgy and the Design of Steels, ed. by Applied Science Publishers LTD, London, (1978), 24.

LIST OF TABLE CAPTIONS

Table 1. Chemical composition of the steel used (mass contents in %).

Table 2. Lattice parameters of ferrite (α) and austenite (γ) and of the orthorhombic phase cementite (θ) as a function of temperature T (K) and the atomic fraction of carbon (ξ). [7,20-23]

Table 3. Values of critical temperatures (ºC) determined by dilatometry.

Table 4. Percentages of ferrite and pearlite measured by image analyser (IA), lever rule (LR) and Kop et al. method (Kop)

Table 5. Values of parameter $t_{0.5}$ and exponent n in expression (7).

LIST OF FIGURE CAPTIONS

Fig. 1. (a) Dilatometric curve for given cooling and heating rates; (b) microstructure of ferrite and pearlite corresponding to dilatometric test.

Fig. 2. (a) Dilatometric curve for given cooling and heating rates; (b) microstructure of ferrite and pearlite corresponding to dilatometric test.

Fig. 3. (a) Dilatometric curve for given cooling and heating rates; (b) microstructure of ferrite and pearlite corresponding to dilatometric test.

Fig. 4. (a) Dilatometric curve for given cooling and heating rates; (b) microstructure of ferrite and pearlite corresponding to dilatometric test.

Fig. 5. Cooling Rate dependence of the initial ($(A'_{r1})_s$) and final ($(A'_{r1})_f$) eutectoid transformation temperatures, showing the intersection of regressions at 707 ºC.

Fig. 6. Lever-rule method.

Fig. 7. Transformed austenite fraction calculated by lever-rule method at given cooling rate.

Fig. 8. Transformed austenite fraction calculated by lever-rule method at given cooling rate.

Fig. 9. Transformed austenite fraction calculated by lever-rule method at given cooling rate.

Fig. 10. Transformed austenite fraction calculated by lever-rule method at given cooling rate.

Fig. 11. Fraction curves obtained from lever-rule and Kop et al. method at given cooling rate.

Fig. 12. Fraction curves obtained from lever-rule and Kop et al. method at given cooling rate.

Fig. 13. Fraction curves obtained from lever-rule and Kop et al. method at given cooling rate.

Fig. 14. Fraction curves obtained from lever-rule and Kop et al. method at given cooling rate.

Fig. 15. Comparison of pearlite fraction calculated from both methods and the pearlite fracction measured by Image Analysis for the different cooling rates used.

Fig. 16. Proeutectoid ferrite fraction calculated by Kop et al. method against time, for different cooling rates used (scatter graphs). The model for phase transformation kinetics based on Avrami's Law is also plotted (solid lines).

Fig. 17. Parameter $t_{0.5}$ of transformation kinetics model against the inverse of cooling rate.

Table 1. Chemical composition of the steel used (mass contents in %).

C	Si	Mn	P	S	Nb	Al	Cu	Cr	N	O
0.09	0.23	1.1	0.021	0.007	0.017	0.005	0.015	0.066	0.017	0.0057

Table 2. Lattice parameters of ferrite (α) and austenite (γ) and of the orthorhombic phase cementite (θ) as a function of temperature T (K) and the atomic fraction of carbon (ξ). [7,20-23]

Phase	Lattice parameters (Å)
α	$a_\alpha = 2.8863\ [1 + 17.5 \cdot 10^{-6}(T - 800)]$ Temperature range (K): $800<T<1200$
γ	$a_\gamma = (3.6306 + 0.78\xi) \cdot [1 + (24.9 - 50\xi) \cdot 10^{-6}(T - 1000)$ Temperature range (K): $1000<T<1250$ Range of atomic fraction of carbon: $0.0005<\xi<0.0365$
θ	$a_\theta = 4.5234[1 + (5.311 \cdot 10^{-6} - 1.942 \cdot 10^{-9}T + 9.655 \cdot 10^{-12}T^2)(T - 293)]$ $b_\theta = 5.0883[1 + (5.311 \cdot 10^{-6} - 1.942 \cdot 10^{-9}T + 9.655 \cdot 10^{-12}T^2)(T - 293)]$ $c_\theta = 6.7426[1 + (5.311 \cdot 10^{-6} - 1.942 \cdot 10^{-9}T + 9.655 \cdot 10^{-12}T^2)(T - 293)]$ Temperature range (K): $300<T<1000$

Table 3. Values of critical temperatures (ºC) determined by dilatometry.

Cooling rate, ºC/s	A'_{r3}	A_{r3}	A_{r1}	$(A'_{r1})_s$	$(A'_{r1})_f$
1.25	809	784	710	634	589
0.84	818	791	722	642	595
0.42	829	800	727	649	610
0.25	842	808	745	656	623

Table 4. Percentages of ferrite and pearlite measured by image analyser (IA), lever rule (LR) and Kop et al. method (Kop)

Cooling rate, °C/s	IA		LR		Kop	
	Ferrite, %	Pearlite, %	Ferrite, %	Pearlite, %	Ferrite, %	Pearlite, %
0.25	83	17	95.9	4.1	87.8	12.2
0.42	87.3	12.7	96.6	3.4	87.7	12.3
0.84	88.2	11.8	96.5	3.5	87.6	12.4
1.25	89.2	10.8	97.2	2.8	87.9	12.1

Table 5. Values of parameter $t_{0.5}$ and exponent n in expression (7).

Cooling rate, ºC/s	$t_{0.5}$, s	n
0.25	273.0	2.05
0.42	161.9	2.06
0.84	75.1	2.07
1.25	49.9	2.06

(a)

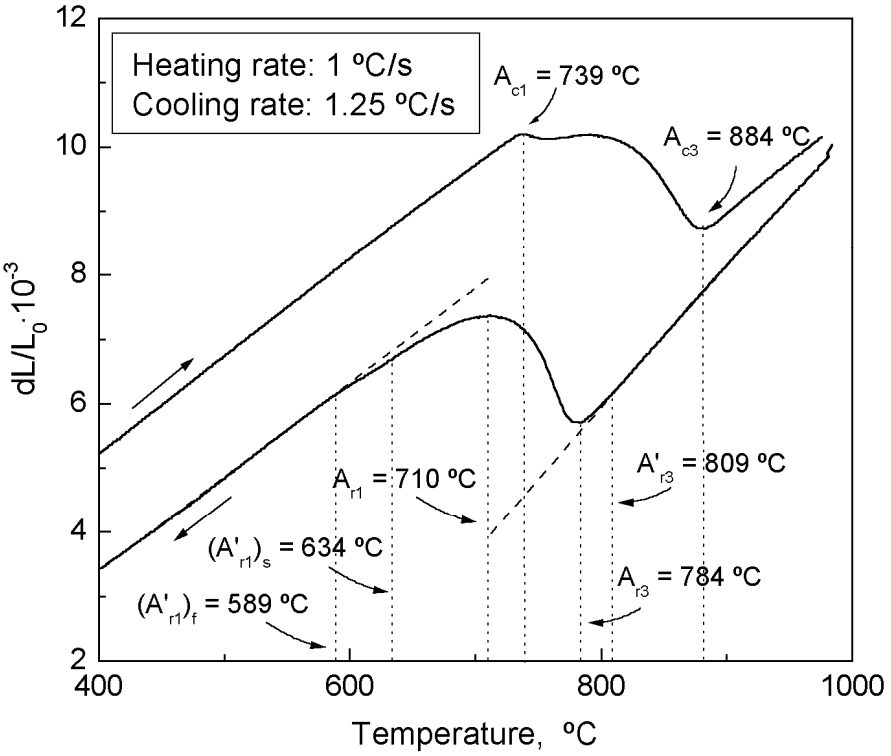

(b)

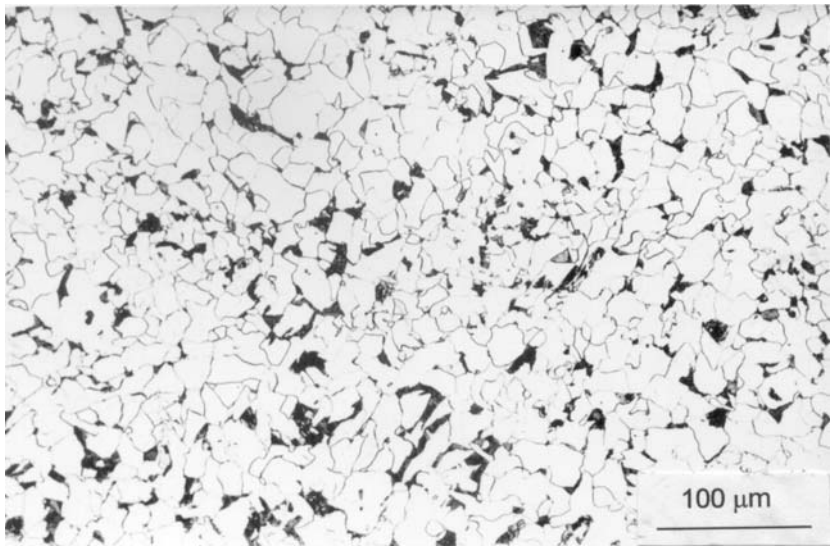

Fig. 1. (a) Dilatometric curve for given cooling and heating rates; (b) microstructure of ferrite and pearlite corresponding to dilatometric test.

(a)

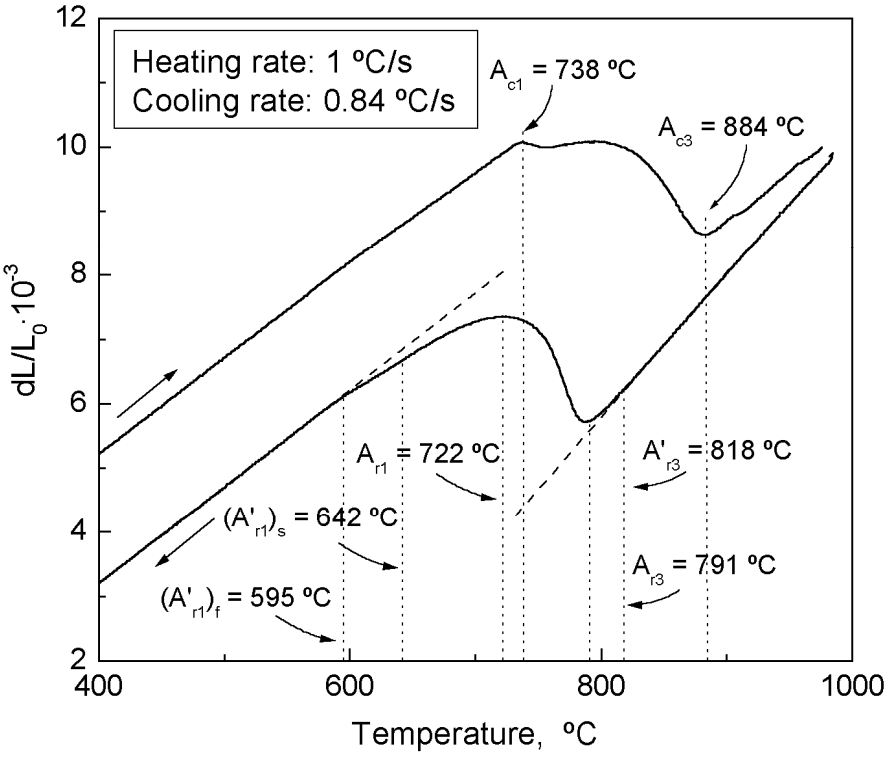

(b)

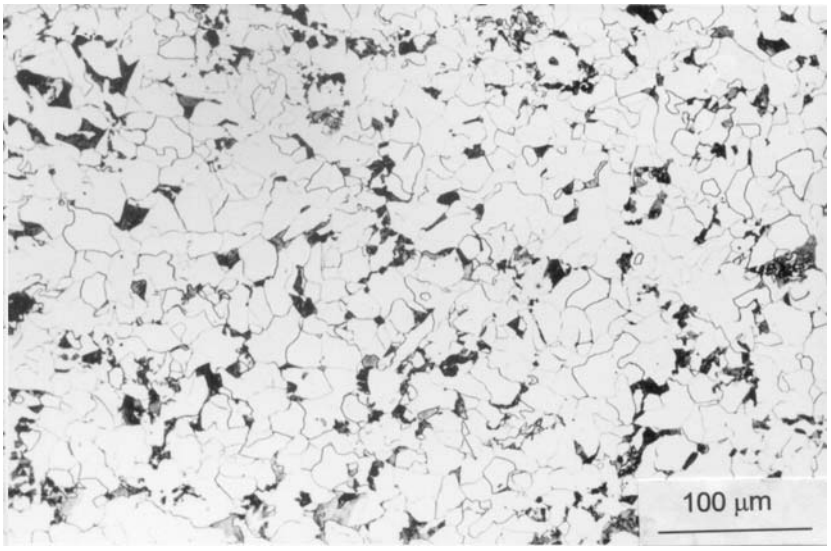

Fig. 2. (a) Dilatometric curve for given cooling and heating rates; (b) microstructure of ferrite and pearlite corresponding to dilatometric test.

(a)

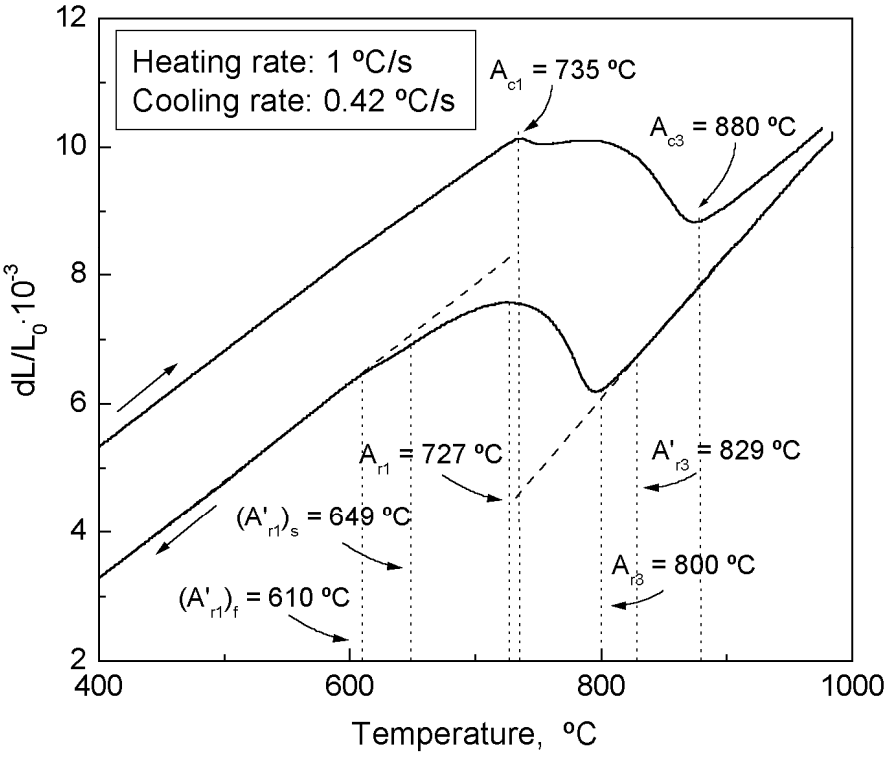

(b)

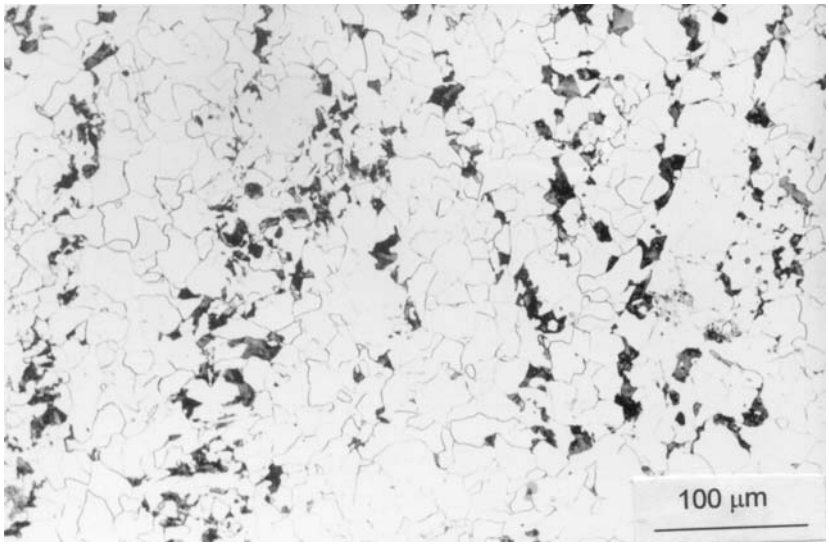

Fig. 3. (a) Dilatometric curve for given cooling and heating rates; (b) microstructure of ferrite and pearlite corresponding to dilatometric test.

(a)

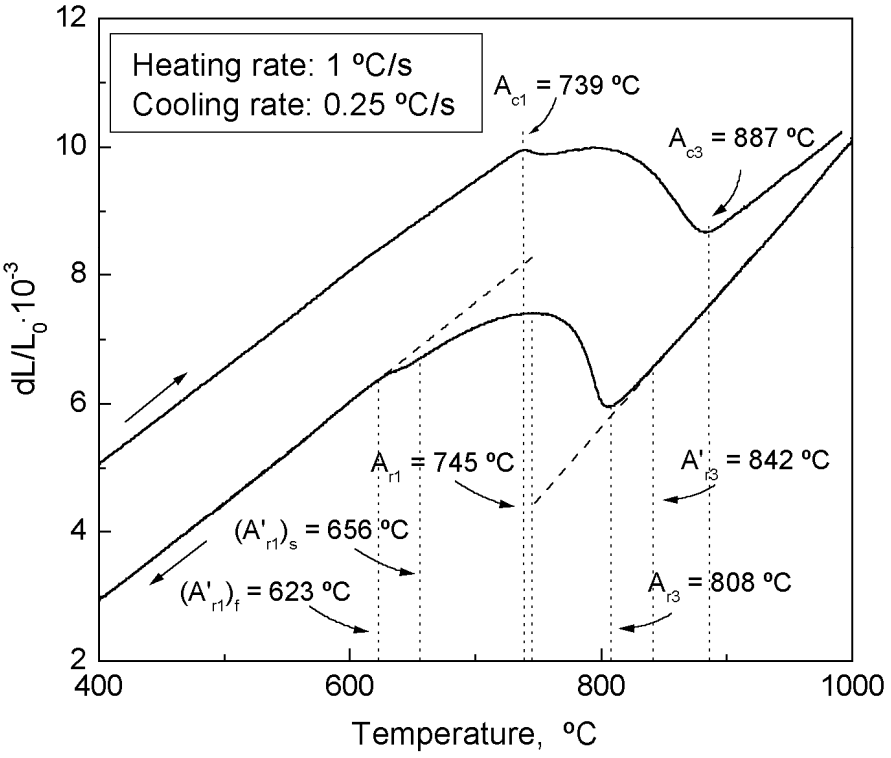

(b)

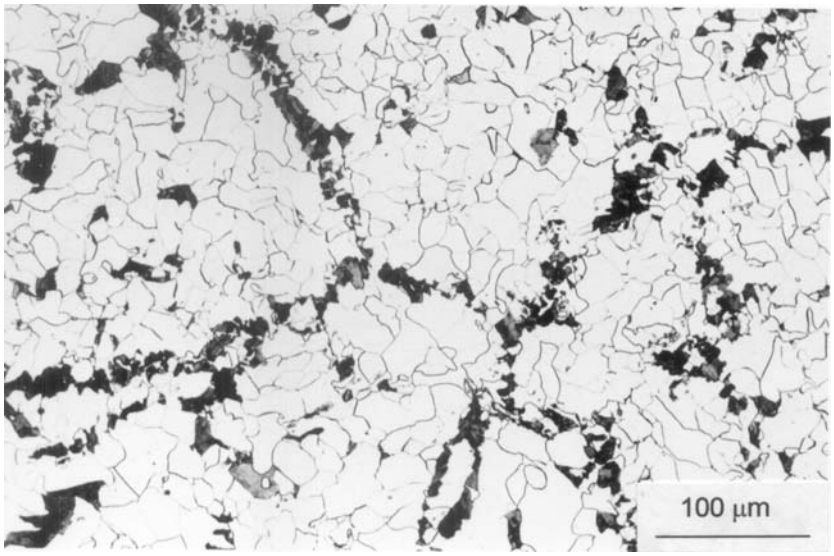

Fig. 4. (a) Dilatometric curve for given cooling and heating rates; (b) microstructure of ferrite and pearlite corresponding to dilatometric test.

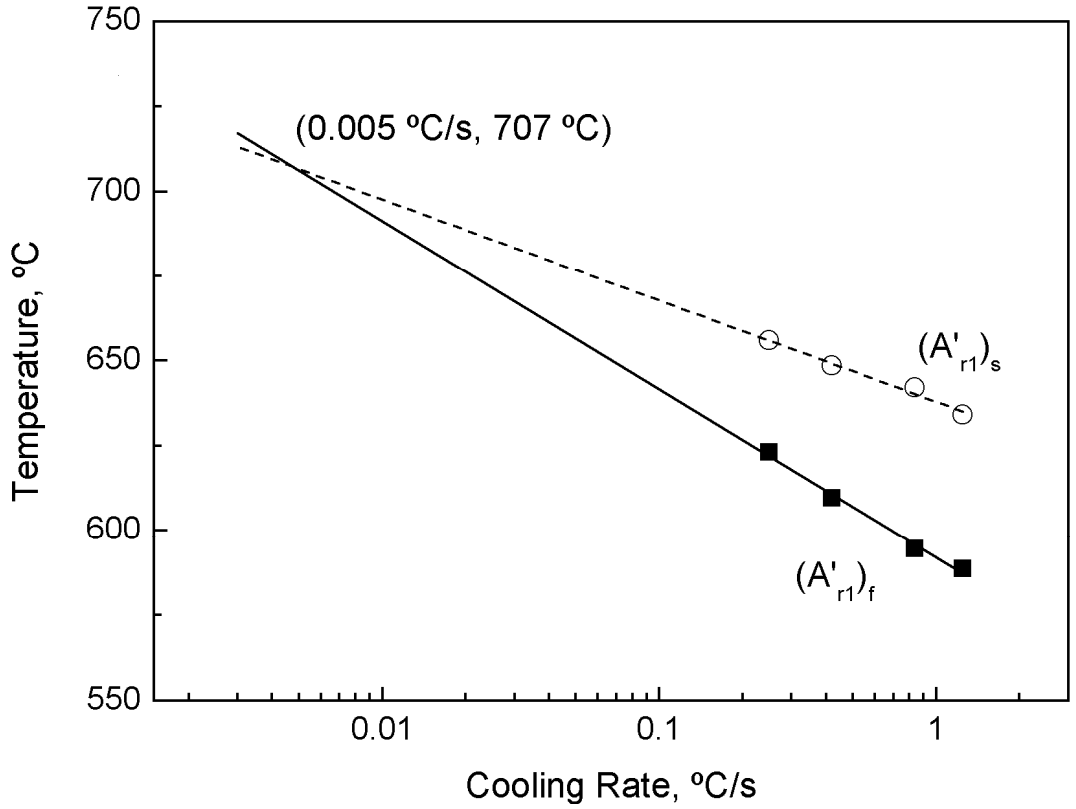

Fig. 5. Cooling Rate dependence of the initial ($(A'_{r1})_s$) and final ($(A'_{r1})_f$) eutectoid transformation temperatures, showing the intersection of regressions at 707 ºC.

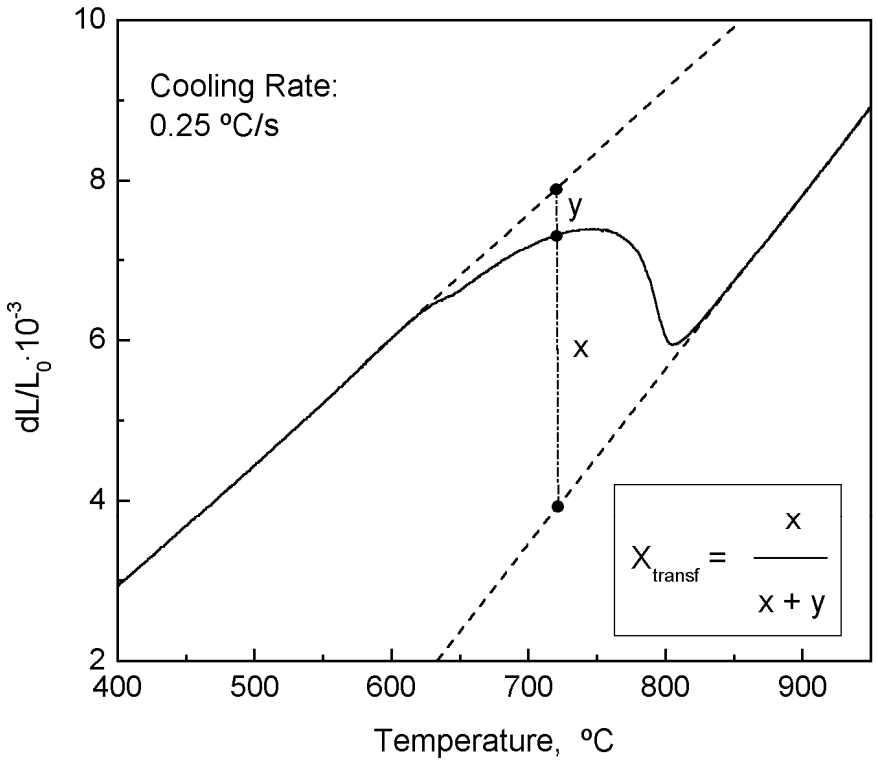

Fig. 6. Lever-rule method.

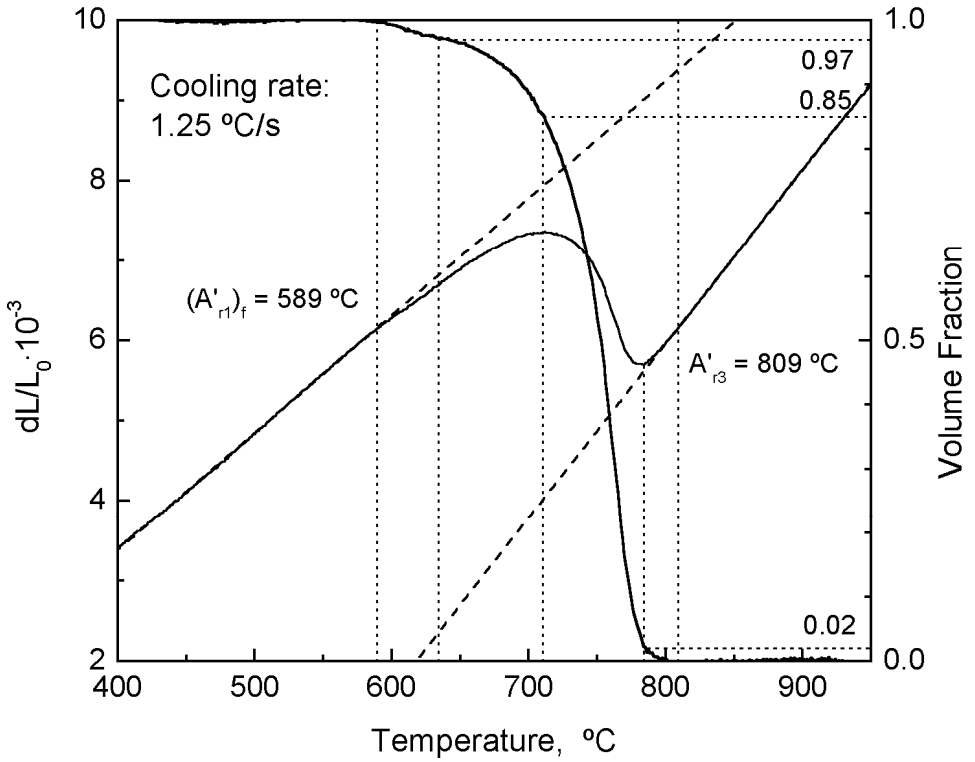

Fig. 7. Transformed austenite fraction calculated by lever-rule method at given cooling rate.

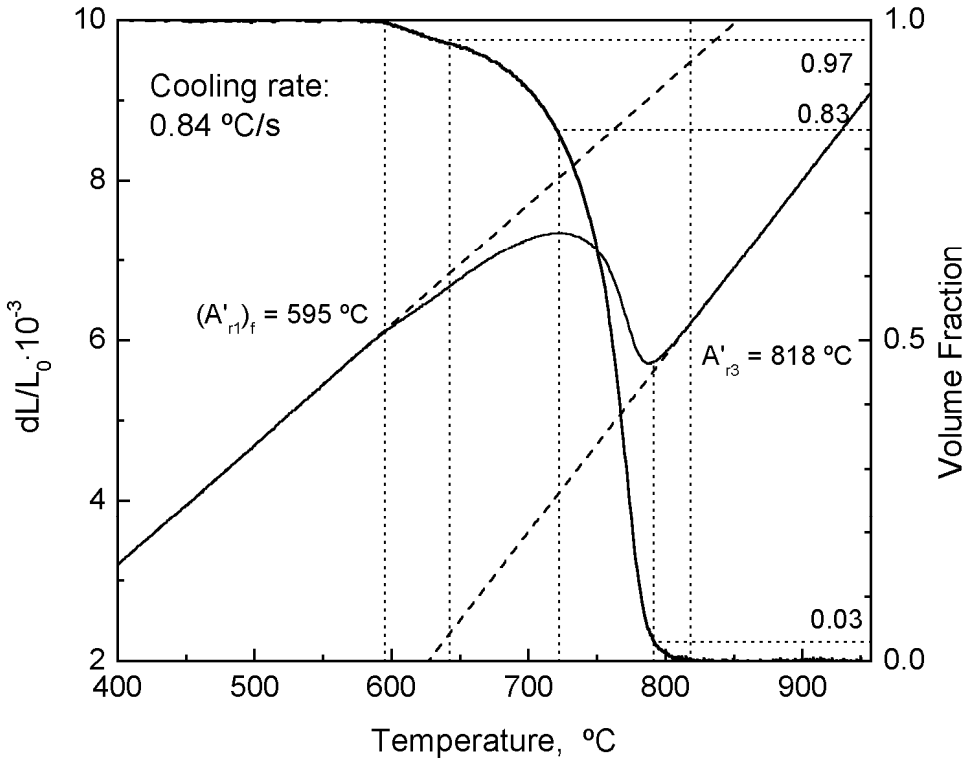

Fig. 8. Transformed austenite fraction calculated by lever-rule method at given cooling rate.

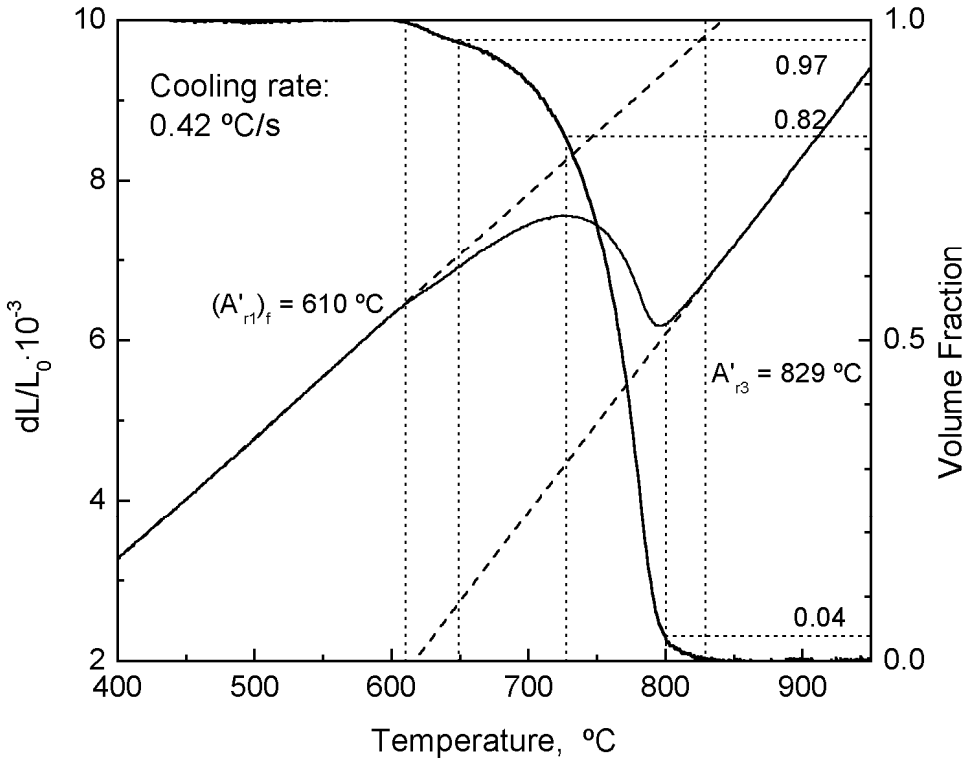

Fig. 9. Transformed austenite fraction calculated by lever-rule method at given cooling rate.

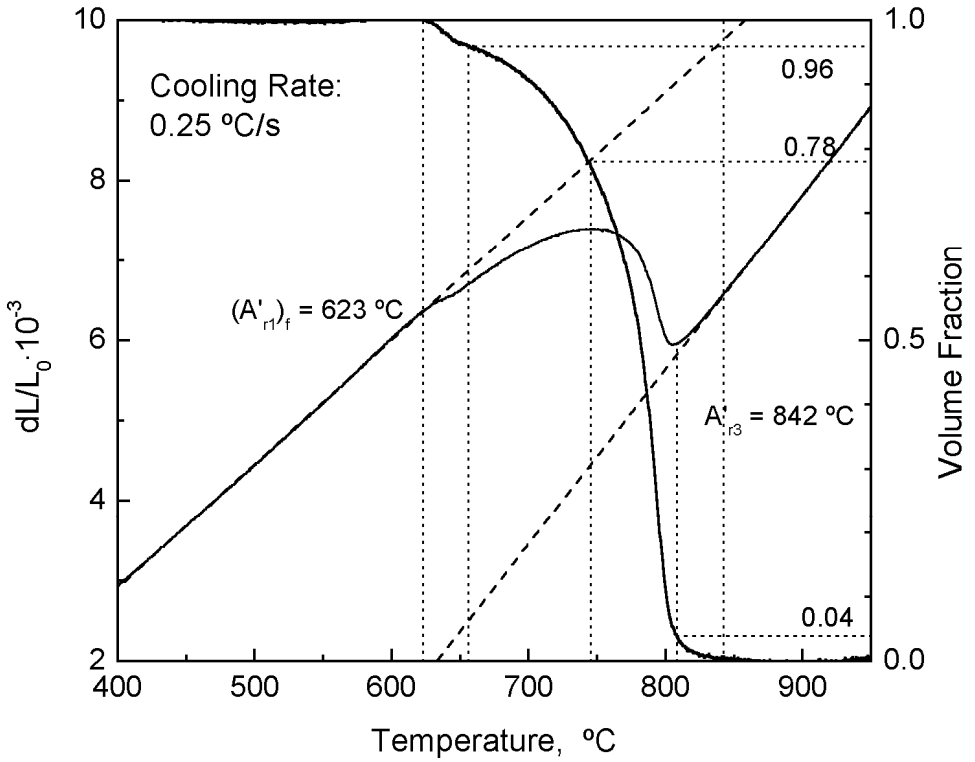

Fig. 10. Transformed austenite fraction calculated by lever-rule method at given cooling rate.

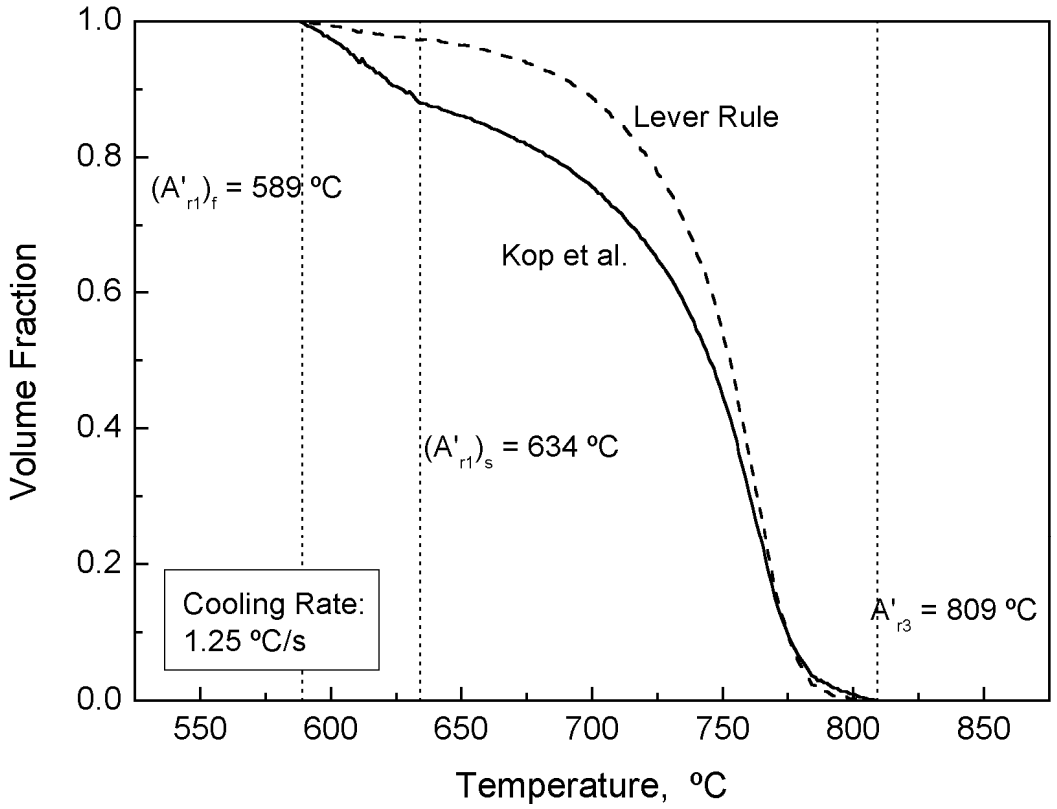

Fig. 11. Fraction curves obtained from lever-rule and Kop et al. method at given cooling rate.

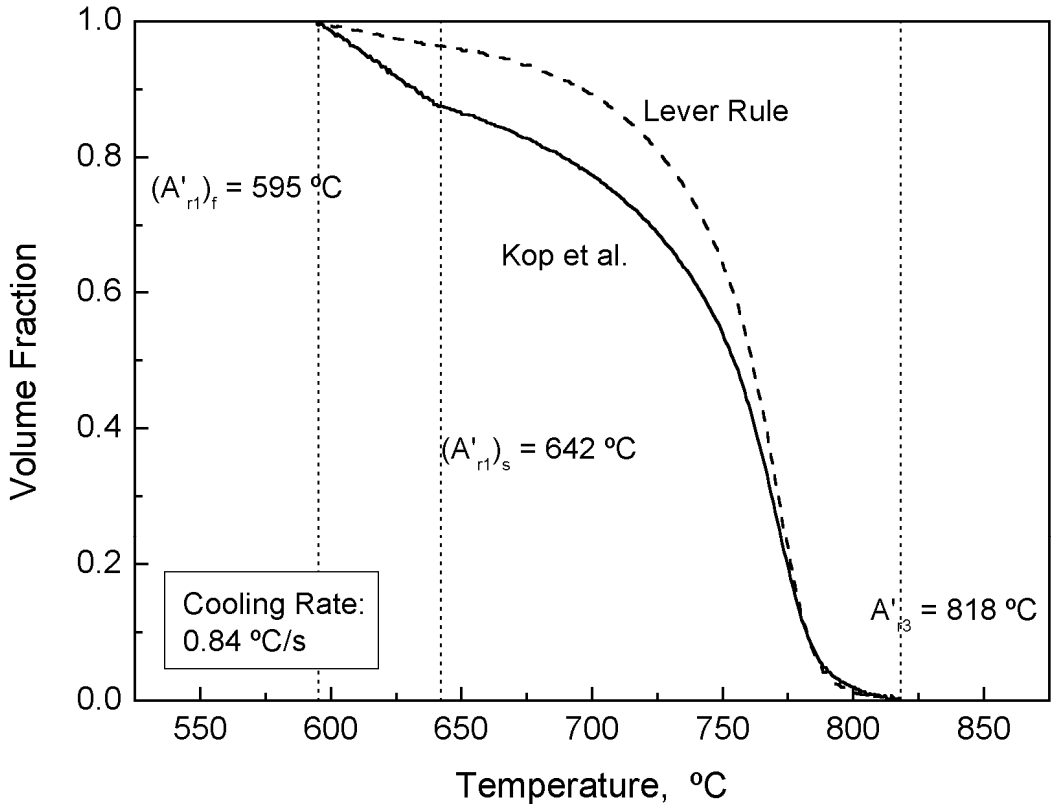

Fig. 12. Fraction curves obtained from lever-rule and Kop et al. method at given cooling rate.

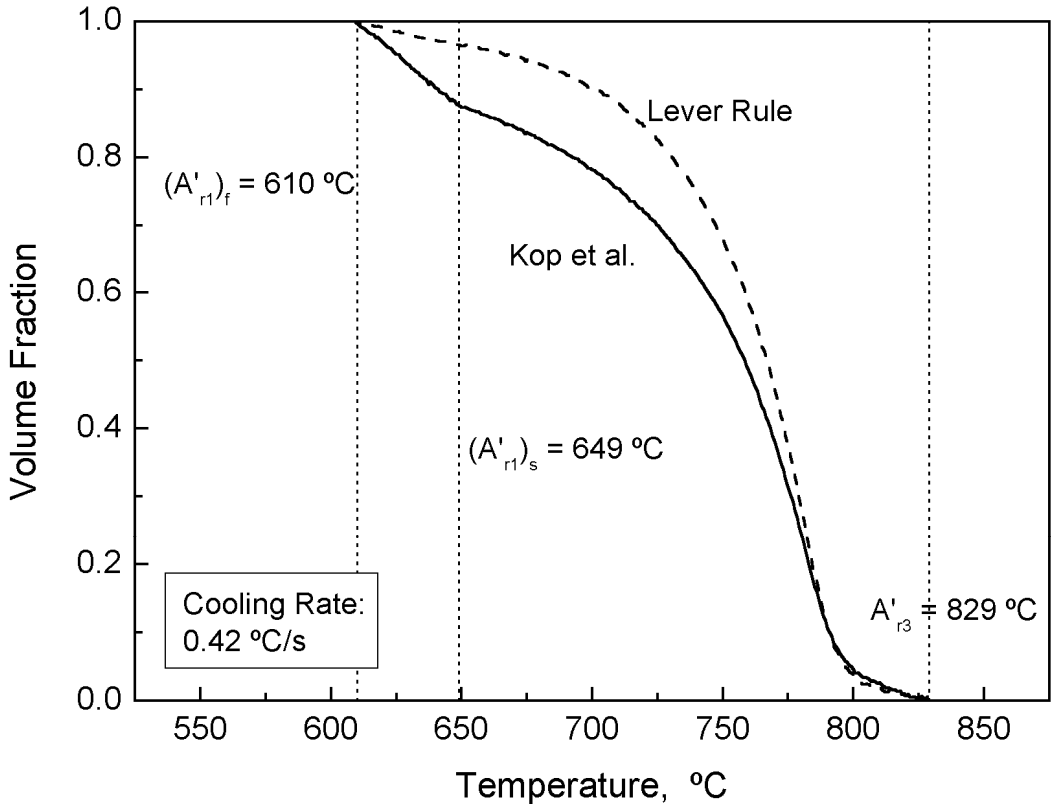

Fig. 13. Fraction curves obtained from lever-rule and Kop et al. method at given cooling rate.

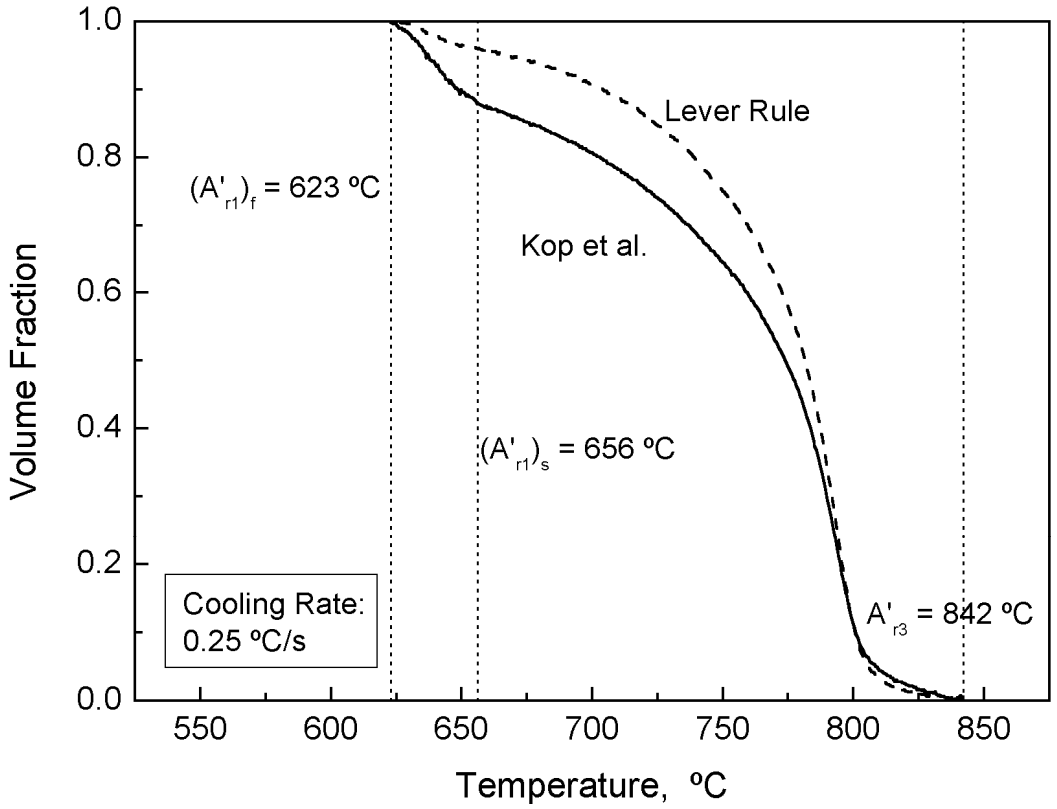

Fig. 14. Fraction curves obtained from lever-rule and Kop et al. method at given cooling rate.

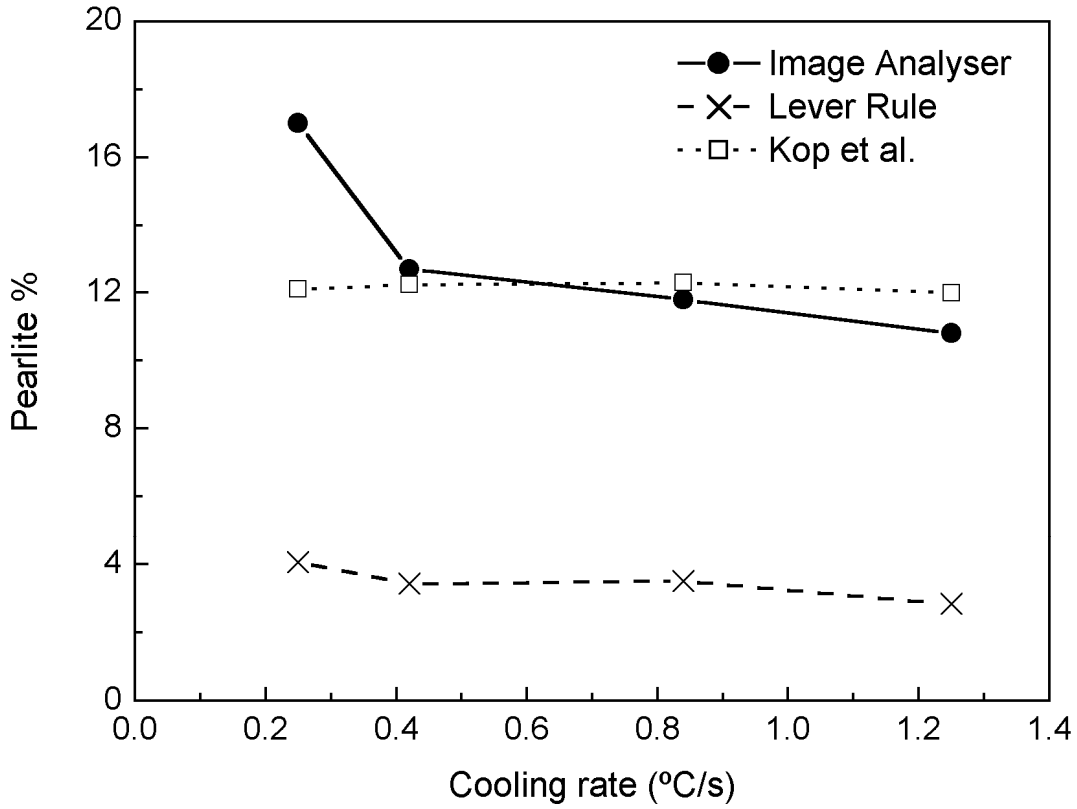

Fig. 15. Comparison of pearlite fraction calculated from both methods and the pearlite fraction measured by Image Analysis for the different cooling rates used.

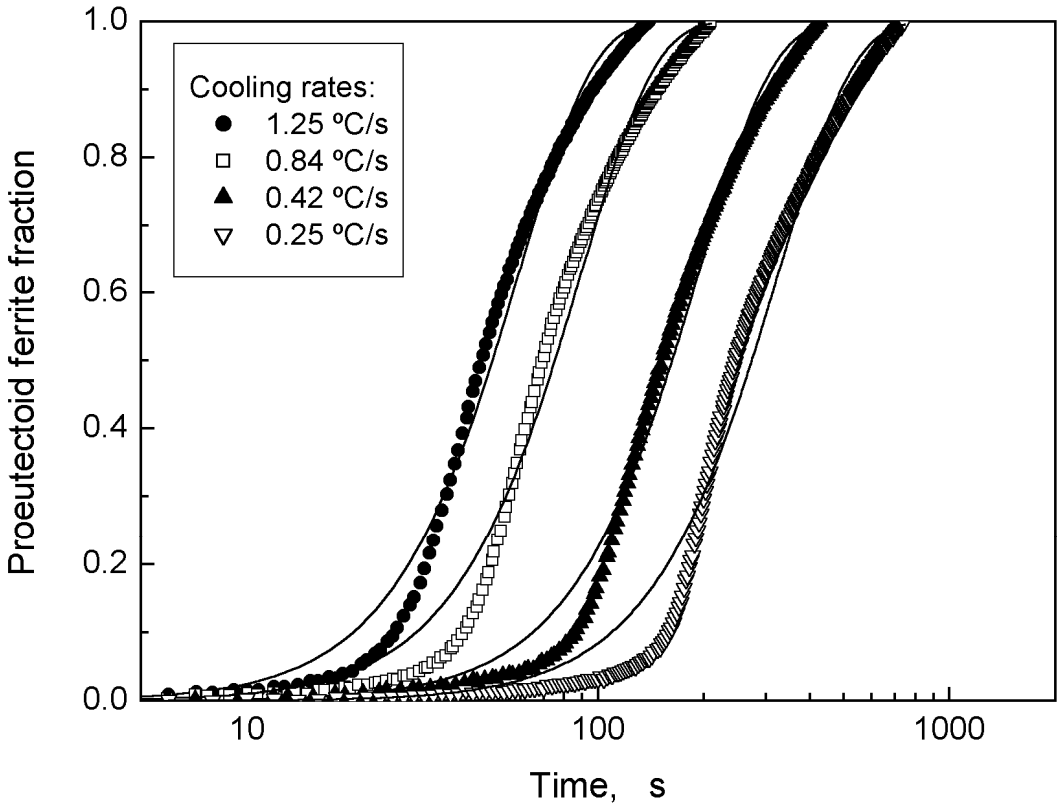

Fig. 16. Proeutectoid ferrite fraction calculated by Kop et al. method against time, for different cooling rates used (scatter graphs). The model for phase transformation kinetics based on Avrami's Law is also plotted (solid lines).

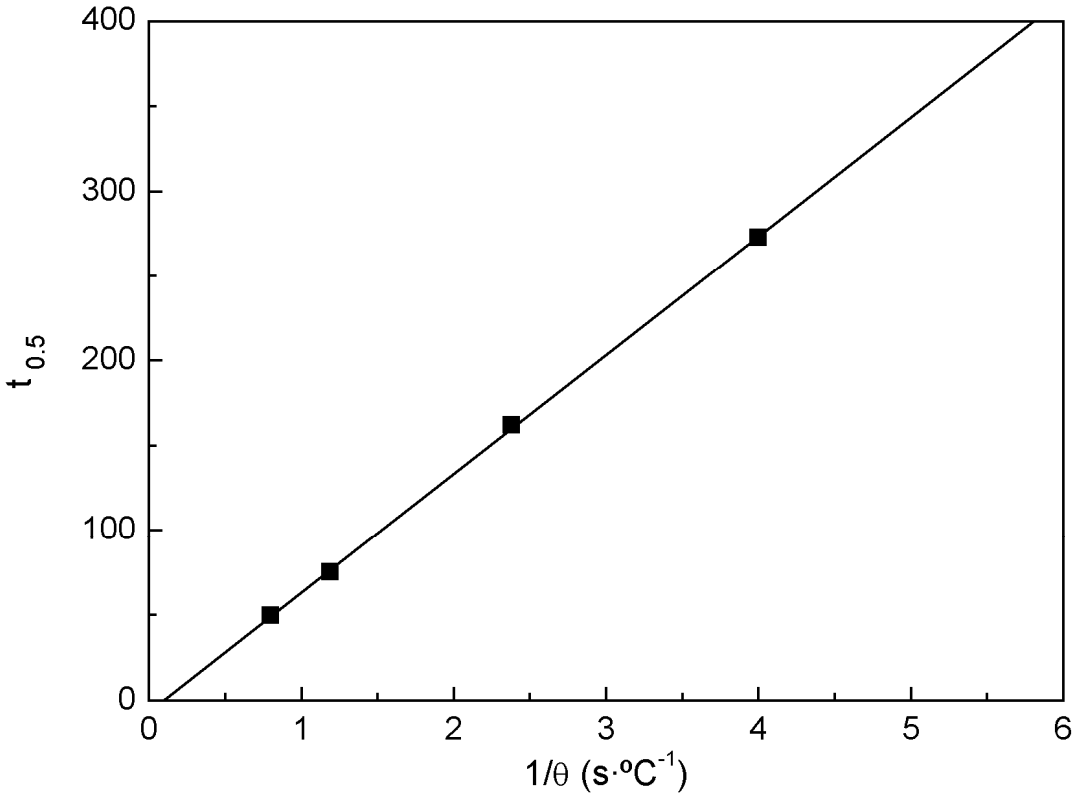

Fig. 17. Parameter $t_{0.5}$ of transformation kinetics model against the inverse of cooling rate.